ACS APPLIED NANO MATERIALS
Cite This: ACS Appl. Nano Mater. 2018, 1, 5655−5661
Article
www.acsanm.org

Stepwise Sulfurization from MoO_3 to MoS_2 via Chemical Vapor Deposition

Joshua V. Pondick,[†,‡] John M. Woods,[†,‡] Jie Xing,[§] Yu Zhou,[∥] and Judy J. Cha*[,†,‡,⊥]

[†]Department of Mechanical Engineering and Materials Science, Yale University, New Haven, Connecticut 06511, United States
[‡]Energy Sciences Institute, Yale University West Campus, West Haven, Connecticut 06516, United States
[§]College of Materials Science and Engineering, Sichuan University, Chengdu 610065, People's Republic of China
[∥]Department of Applied Physical Sciences, University of North Carolina at Chapel Hill, Chapel Hill, North Carolina 27514, United States

Supporting Information

ABSTRACT: Chemical vapor deposition (CVD) is used widely to synthesize monolayer and few-layer transition metal dichalcogenide molybdenum disulfide (MoS_2), a two-dimensional (2D) material with various applications in nanoelectronics, catalysis, and optoelectronics. However, the CVD synthesis of 2D MoS_2 is highly sensitive to small changes in growth parameters and the growth mechanism has not been extensively studied. This work systematically investigates the effect of sulfur concentration on CVD synthesis of MoS_2 using molybdenum trioxide (MoO_3) and sulfur precursors. We find that with increasing concentration of sulfur vapor, intermediate products of molybdenum dioxide (MoO_2) and molybdenum oxysulfide ($MoOS_2$) can form during a stepwise sulfurization of MoO_3 to the final product of MoS_2. The intermediate $MoOS_2$, formed due to sulfur vapor deficiency, can be fully converted to MoS_2 with further sulfurization. We show that the local sulfur to molybdenum vapor ratio at the growth substrate critically determines the growth products. This study thus highlights the importance of keeping the molar ratio of sulfur to molybdenum vapor well in excess of the stoichiometrically required ratio of 3.5:1 in order to grow 2D MoS_2.

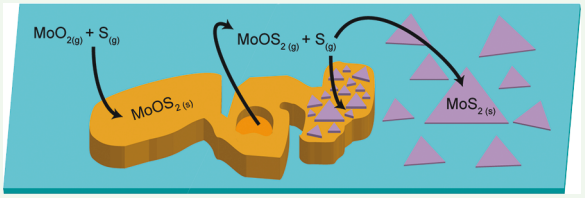

KEYWORDS: *molybdenum disulfide, chemical vapor deposition, sulfurization, growth mechanism, molybdenum oxysulfide, molybdenum oxide*

Atomically thin transition metal dichalcogenides (TMDs) are two-dimensional (2D) materials with the formula MX_2, where M is a transition metal and X is a chalcogen, such as S, Se, or Te. They have been the subject of great interest due to their physical, chemical, and electronic properties with applications for field-effect transistors,[1−3] optoelectronic devices,[4−6] and catalysis.[7−10] The layer-dependent bandgap and attractive mechanical properties of the semiconducting TMD molybdenum disulfide (MoS_2) have created a demand for high-quality 2D crystals of MoS_2.[11,12] A number of synthesis techniques have yielded thin MoS_2, including mechanical exfoliation,[11,12] chemical exfoliation via intercalation,[13−16] and molecular beam epitaxy;[17] however the demand for controllable size, thickness, morphology, and scalability has led to the dominance of chemical vapor deposition. Chemical vapor deposition (CVD) is widely used to grow continuous thin films[18−23] and triangular flakes,[24−29] but the challenging nature of CVD continues to stimulate insightful research into the improvement of the technique. Recent works, such as the controlled growth of MoS_2 nanoribbons,[30] the synthesis of a large range of 2D TMDs via molten-salt assisted CVD growth,[31] and in situ microscopy of the formation of edge-terminated MoS_2 on MoO_2 nanocrystals,[32] have demonstrated the importance of understanding the growth mechanism. Additionally, ab initio calculations of the defect density of synthesized MoS_2 indicate that CVD minimizes defects detrimental for electronic applications, further highlighting the importance of studying the CVD growth process.[33] The effects of pressure,[34] temperature,[22,26,34−36] flow rate,[35] substrate seeding,[19,29,37] reaction geometry,[22,25,26,36−38] and Mo precursor concentration[31,38,39] have been exhaustively studied with the aim of controlling the morphology and size of CVD-grown MoS_2. However, the role of sulfur concentration on MoS_2 growth has not been as extensively studied as other growth parameters.

Elemental sulfur (S) and molybdenum trioxide (MoO_3) powders are commonly used precursors for the CVD-growth of MoS_2 via the following sulfurization reaction:

$$2MoO_{3(g)} + 7S_{(g)} \rightarrow 2MoS_{2(s)} + 3SO_{2(g)} \quad (1)$$

The sulfur concentration is important in this reaction, with hexagonal or triangular MoS_2 flakes grown in sulfur deficient or excess conditions, respectively.[34,38] In addition, incomplete sulfurization of MoO_3 can lead to the formation of

Received: July 23, 2018
Accepted: September 12, 2018
Published: September 12, 2018

DOI: 10.1021/acsanm.8b01266
ACS Appl. Nano Mater. 2018, 1, 5655−5661

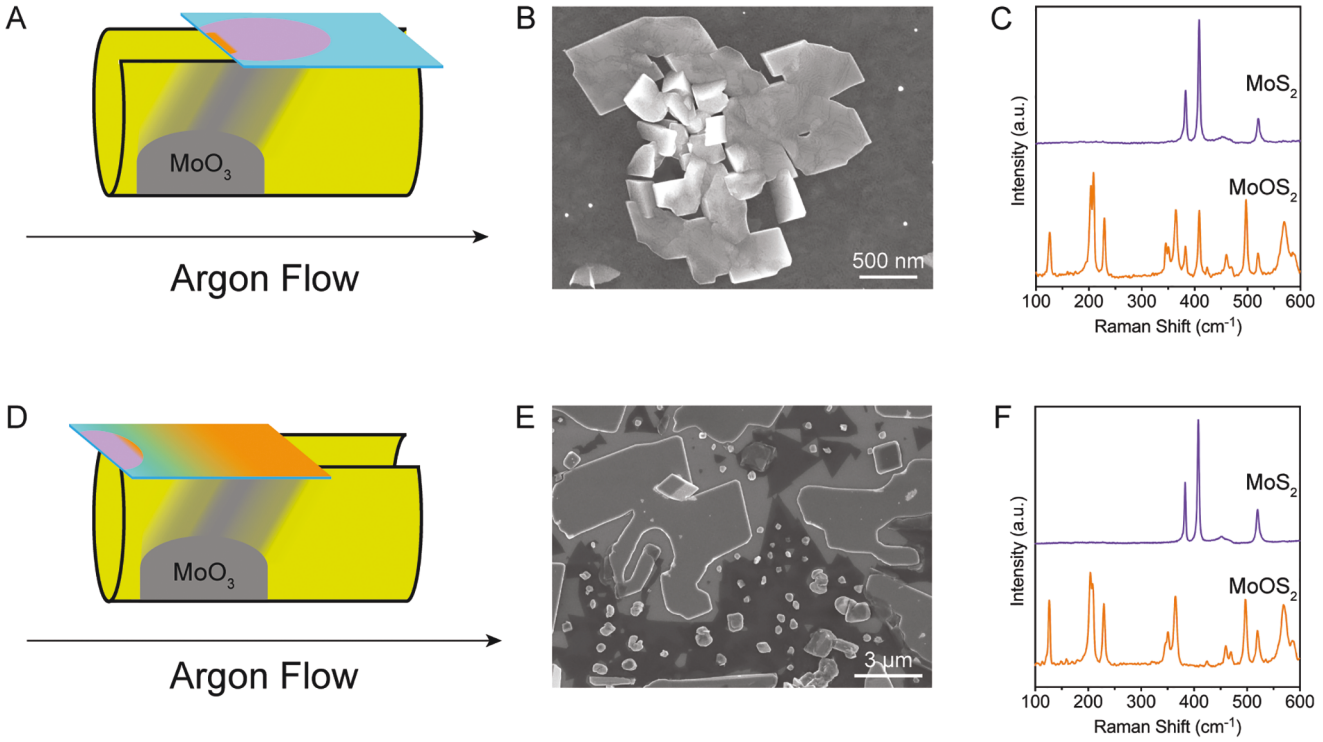

Figure 1. Local fluctuations in S:Mo ratio lead to the growth of intermediates. (A) Schematic diagram of locally increased Mo concentration at the leading edge of a substrate. On the substrate surface, blue, orange, and purple correspond to SiO_2, $MoOS_2$, and MoS_2, respectively. Beneath the substrate, yellow represents sulfur vapor and gray represents Mo vapor. (B) SEM image of $MoOS_2$ crystals formed at the front edge of the substrate. (C) Raman spectra of the MoS_2 film (top) and $MoOS_2$ crystals (bottom). The peak at 520 cm^{-1} corresponds to the Si growth substrate. (D) Schematic diagram of locally decreased Mo concentration at the leading edge of a substrate. On the substrate surface, blue, orange, and purple correspond to SiO_2, $MoOS_2$, and MoS_2, respectively. Beneath the substrate, yellow represents sulfur vapor and gray represents Mo vapor. (E) SEM image of triangular MoS_2 crystals growing between $MoOS_2$ crystals. (F) Raman spectra of the MoS_2 crystals (top) and $MoOS_2$ crystals (bottom). The peak at 520 cm^{-1} corresponds to the Si growth substrate.

molybdenum oxides (MoO_{3-x})[40−43] and molybdenum oxysulfides ($MoO_{3-x}S_y$; $0 \le x \le 3$; $0 \le y \le 2$).[44,45] While the effect of sulfur concentration on the CVD growth of these intermediates and MoS_2 has been previously reported,[34,38] a systematic investigation of the complete reaction pathway from MoO_3 to MoS_2 during the CVD process has yet to be undertaken. The lack of consensus as to the optimal growth parameters increases the necessity for a thorough understanding of the sulfurization mechanism in order to avoid the undesirable growth of molybdenum oxides and oxysulfides.

In this study, we report the effect of sulfur concentration on the CVD-growth of MoS_2. By varying the local and global sulfur concentrations across the growth substrate surface, we selectively grow molybdenum dioxide (MoO_2), $MoOS_2$, and MoS_2. Chemical and structural characterization of these species reveals a stepwise sulfurization mechanism to convert MoO_3 into MoS_2. The direct observation of hybrid oxysulfide/sulfide species and the conversion of $MoOS_2$ crystals into MoS_2 reveal a growth mechanism whereby oxysulfides can serve as crystalline intermediates that are sulfurized to form MoS_2. Our results demonstrate that to grow MoS_2 and avoid contaminating intermediate species via CVD, maintaining an excess of sulfur vapor is necessary to push the sulfurization of MoO_3 to completion.

RESULTS AND DISCUSSION

The CVD-growth of MoS_2 on a SiO_2 substrate was studied using MoO_3 and sulfur powder precursors placed inside a single-zone tube furnace as outlined in Figure S1 in Supporting Information. The reaction proceeds as a stepwise sulfurization process described by three intermediate reactions:

$$2MoO_3 + S \rightarrow 2MoO_2 + SO_2 \quad (2)$$

$$2MoO_2 + 5S \rightarrow 2MoOS_2 + SO_2 \quad (3)$$

$$2MoOS_2 + S \rightarrow 2MoS_2 + SO_2 \quad (4)$$

In reaction 2, sulfur binds to oxygen to form SO_2 gas and a MoO_2 intermediate. The removal of a second oxygen and formation of two S−Mo bonds in reaction 3 yield an oxysulfide species, $MoOS_2$. The further removal of an oxygen from $MoOS_2$ yields MoS_2. Since both intermediate species are stable, incomplete sulfurization will lead to the formation of solid MoO_2 or $MoOS_2$. The oxide intermediate has been observed in the sulfurization of MoO_3 by H_2S gas,[40] and the oxysulfide intermediate has also been observed.[34,38,45] In total, reaction 1 requires a stoichiometric ratio of 3.5 mol of S to 1 mol of Mo to completely form MoS_2.

The gas-phase reaction of sulfur and MoO_3 vapors is controlled by the local effective molar ratio of S:Mo at the substrate surface. The effective molar ratio at the leading edge of the substrate can be modified by changing the placement of the precursors in relation to the substrate. We fixed the global S:Mo molar loading ratio at 227:1 to grow MoS_2 and placed the substrate 8 mm downstream of the MoO_3 powder (Figure 1A). This geometry lowers the S:Mo molar ratio at the leading edge of the substrate because it is closest to the MoO_3 powder.

DOI: 10.1021/acsanm.8b01266
ACS Appl. Nano Mater. 2018, 1, 5655−5661

While a MoS_2 thin film grew across most of the substrate, small crystals were found within 100 μm of the front edge of the substrate closest to the MoO_3 precursor. These small crystals are irregularly shaped polyhedra (scanning electron micrograph (SEM), Figure 1B), which is uncharacteristic of MoS_2 crystals.[24−29] The Raman spectrum of the small crystals (Figure 1C, bottom) shows the E_{2g} and A_{1g} peaks of MoS_2 [46,47] but also contains a number of peaks that cannot be attributed to the MoO_3 or S precursors (Figure S2). These peaks are consistent with reported spectra of $MoOS_2$ [34,38] and can be attributed to Raman modes arising from vibrations of Mo−S and Mo−O bonds (Table S1),[48−52] revealing these small crystals to be the intermediate $MoOS_2$. The Raman spectrum of the surrounding film shows the expected MoS_2 spectrum (Figure 1C, top).[46,47] This indicates that despite the globally high S:Mo molar ratio, the S:Mo molar ratio can change locally across the substrate due to the poor vapor transport of MoO_3.

To test the opposite effect, we fixed the global S:Mo molar loading ratio at 17:1 to favor the growth of the intermediate product $MoOS_2$ and placed the substrate directly over the MoO_3 powder (Figure 1D). Due to the flow of carrier gas, the MoO_3 vapor was pushed toward the center and far edge of the substrate, leading to a locally increased S:Mo molar ratio at the front edge of the substrate. Consequently, despite the low S:Mo molar loading ratio, MoS_2 clusters still formed at the front edge of the substrate. SEM analysis of the interface between the MoS_2 and $MoOS_2$ in Figure 1E reveals that triangular MoS_2 crystals grew between the irregularly shaped $MoOS_2$ crystals. Raman spectra from the film closest to the front edge of the substrate show the characteristic peaks for MoS_2 (Figure 1F, top), while spectra from the irregular crystals in the interface region show characteristic peaks of $MoOS_2$ (Figure 1F, bottom). The two experiments outlined in Figure 1 demonstrate that local fluctuations in the S:Mo ratio at the substrate surface allow for the formation of products heavily disfavored by the global conditions in the growth furnace.

The effect of the global S:Mo molar ratio was investigated with substrates placed directly above the MoO_3 powder. We changed the constant effective ratio across the substrate surface by varying the amount of sulfur precursor compared to MoO_3. The global S:Mo molar ratio increases with an increasing molar loading ratio, and representative optical images of crystals grown under increasing loading ratios are presented in Figure 2A−C. With a S:Mo molar loading ratio of 3:1, small rhomboid crystals with edge lengths between 1 and 5 μm formed (Figure 2A). The morphology[53] and Raman spectrum of these crystals are consistent with crystalline MoO_2 (Figure 2D top, Table S1).[48,50−55] Under these sulfur-deficient conditions, reaction 2 dominates, favoring the formation of MoO_2. Increasing the S:Mo molar loading ratio to 7:1 yielded large irregularly shaped orange crystals (Figure 2B). The Raman spectrum of these crystals is consistent with that of $MoOS_2$, while the absence of the silicon peak at 520 cm^{-1} indicates that they are thick (Figure 2D middle, Table S1). With the increase in sulfur concentration, both reactions 2 and 3 occur, favoring the formation of $MoOS_2$. Increasing the loading ratio to greater than 200:1 ensured a constant effective S:Mo molar ratio exceeding 3.5:1 throughout the entire growth. This allows for the complete stepwise sulfurization of MoO_3 through reactions 2−4, yielding triangular crystals of MoS_2 (Figure 2C,D bottom, Table S1). Increasing the reaction temperature also changes the global S:Mo ratio by increasing the vapor pressure of MoO_3 and S. We grew continuous films

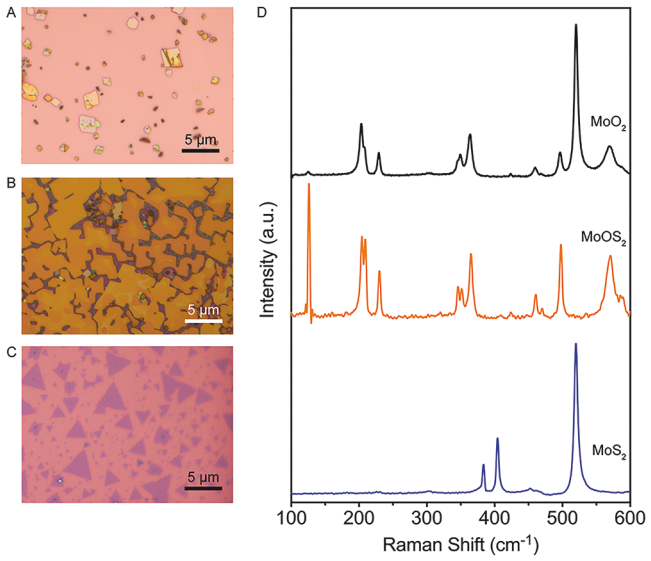

Figure 2. Modulation of global sulfur concentration controls the sulfurization of MoO_3. (A) Optical image of MoO_2 crystals grown under a S:Mo molar loading ratio of 3:1. (B) Optical image of $MoOS_2$ crystals grown under a S:Mo molar loading ratio of 7:1. (C) Optical image of MoS_2 crystals grown under a S:Mo molar loading ratio in excess of 200:1. (D) Raman spectra of the crystals corresponding to MoO_2 (top), $MoOS_2$ (middle), and MoS_2 (bottom). The peak at 520 cm^{-1} corresponds to the Si growth substrate.

of MoS_2 at higher growth temperatures and showed that trace amounts of $MoOS_2$ were still observable at molar loading ratios of 187:1 (Figure S3). This indicates that higher concentrations of MoO_3 vapor were present at higher growth temperatures.

Closer examination of the CVD-grown $MoOS_2$ suggests that $MoOS_2$ can be further sulfurized to form MoS_2. Figure 3A shows a cluster of $MoOS_2$ crystals that display a color gradient, from orange to blue and white. The orange to blue color changing region was examined with SEM, which shows the optical color change as contrast change (Figure 3B). Figure 3C reveals triangular growth boundaries at the boundary of the contrast change, indicating the boundary is between the triangular MoS_2 and the intermediate $MoOS_2$. The X-ray photoelectron spectroscopy (XPS) analysis of this cluster is shown in Figures 3D and S4. The O 1s spectrum contains a main peak originating from the SiO_2 substrate[56] but also contains a smaller peak at lower binding energy originating from the Mo−O bonds of $MoOS_2$ (Figure 3D, left).[57] Two overlapping doublets are observed in the Mo 3d spectrum, corresponding to the $3d_{3/2}$ and $3d_{5/2}$ peaks of Mo^{4+} and Mo^{6+} (Figure 3D, right).[58,59] The 4+ oxidation state of Mo suggests that MoS_2 is present in this cluster.[19] The mixture of 4+ and 6+ oxidation states can also indicate the presence $MoOS_2$.[58,59]

To further probe the chemistry of this cluster, a microscope-directed laser was used to collect Raman spectra from 532 nm regions of individual crystals. Raman spectroscopy confirms that the blue-white crystals are MoS_2, while the irregularly shaped orange crystals are $MoOS_2$ (Figure 3E). The Raman spectrum from the purple regions contains all of the peaks from $MoOS_2$ and MoS_2 (Figure 3E). This provides direct evidence for the presence of $MoOS_2/MoS_2$ hybrid crystals in the transition regions. Hybrid crystals were also observed at a S:Mo molar loading ratio of 17:1 in a cluster containing all three species (Figure S5). The triangular growth boundaries

DOI: 10.1021/acsanm.8b01266
ACS Appl. Nano Mater. 2018, 1, 5655−5661

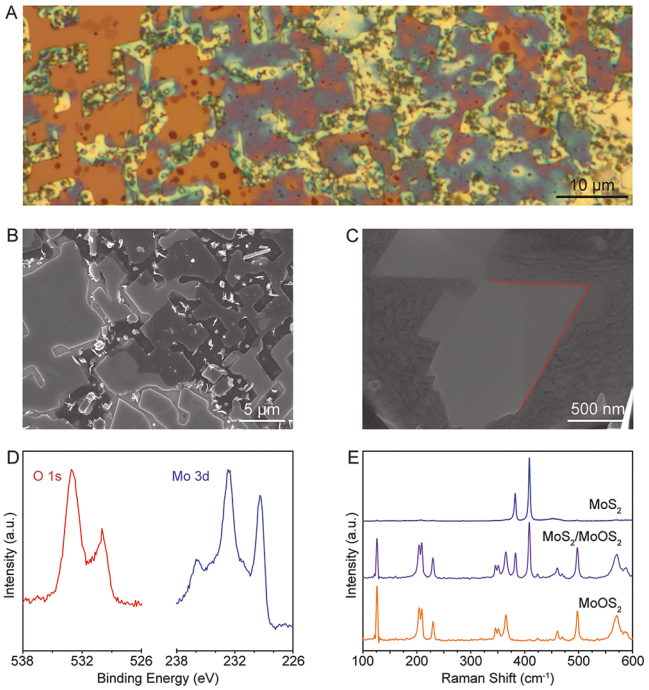

Figure 3. Characterization of $MoOS_2/MoS_2$ hybrid crystals. (A) Optical image of $MoOS_2$ crystals (orange) transitioning to MoS_2 crystals (blue-white). Hybrid $MoOS_2/MoS_2$ crystals are also observed (purple). (B) SEM image of $MoOS_2$ crystals (light) transitioning to MoS_2 (dark). (C) SEM image of the boundary between $MoOS_2$ (light) and MoS_2 (dark). The boundary denoted by the dotted red line highlights the characteristic triangular morphology of MoS_2. (D) XPS spectra of the O 1s peaks (left) and Mo 3d peaks (right) from the cluster shown in (A). (E) Raman spectra of MoS_2 originating from the blue and blue-white crystals (top), hybrid $MoOS_2/MoS_2$ species originating from the interfacial region of orange/purple crystals (middle), and $MoOS_2$ from the orange crystals (bottom).

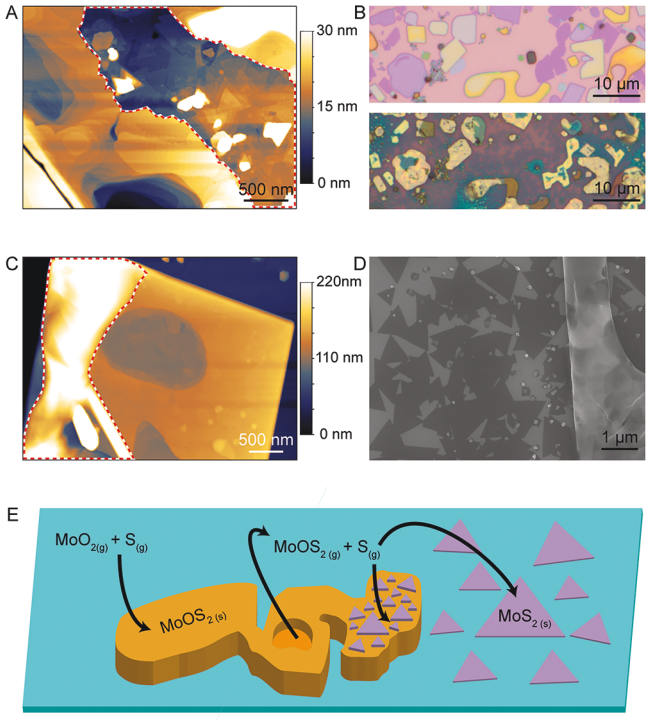

Figure 4. Sulfurization of $MoOS_2$ to form MoS_2. (A) Representative AFM image of the transition region between $MoOS_2$ and MoS_2 (encircled by the red/white dashed line). The MoS_2 region is characterized by the growth of layered triangular crystals, while the $MoOS_2$ region contains deep pits. (B) Optical images of $MoOS_2$ crystals grown under sulfur deficient conditions before (top) and after (bottom) sulfurization. (C) AFM image of the transition region between $MoOS_2$ and MoS_2 in a crystal shown in (B). The region on the left encircled by the red/white dashed line corresponds to MoS_2, while the deep pit and smooth right portion of the crystal correspond to $MoOS_2$. (D) SEM image of triangular MoS_2 crystals growing around the sulfurized crystals in (B). (E) Schematic of the stepwise sulfurization of MoO_3 to form MoS_2 via a crystalline $MoOS_2$ intermediate.

present in the hybrid crystals suggest $MoOS_2$ serves a growth substrate for MoS_2 similar to reported CVD growth of MoS_2 on top of MoO_x under sulfur deficient conditions.[60]

To determine if $MoOS_2$ acts a growth substrate, we analyzed the hybrid crystals using atomic force microscopy (AFM). Figures 4A and S6A show the interface between $MoOS_2$ and MoS_2, revealing deep pits in the $MoOS_2$ surface and layered MoS_2 triangular domains growing next to the $MoOS_2$ pits. These pits are not present in the orange $MoOS_2$ crystals further away from the interfacial region (Figure S6B), and the purple region of MoS_2 is revealed to be comprised of layers of triangular crystals (Figure S6C). The presence of the pits at the interface between $MoOS_2$ and MoS_2 suggests a growth mechanism through which solid $MoOS_2$ is consumed during the adjacent growth of MoS_2. To confirm this mechanism, MoO_3 was sulfurized under sulfur deficient conditions, yielding irregularly shaped orange and purple $MoOS_2$ crystals (Figure 4B top and Figure S7). These crystals were then sulfurized in the absence of any Mo precursor. The crystals shrunk in size and changed color to blue-white (Figure 4B, bottom). Raman spectroscopy confirmed that these blue-white crystals were MoS_2 (Figure S7). A few isolated crystals retained orange regions, which were found to be hybrid $MoOS_2/MoS_2$ species via Raman spectroscopy (Figure S7). Examination of these hybrid regions with AFM revealed deep pits (Figure 4C). SEM and Raman analysis shows that the purple triangular flakes that grew on the substrate during the second sulfurization are MoS_2 (Figures 4D and S7).

On the basis of reaction 4, $MoOS_2$ is an intermediate to the formation of MoS_2, so we propose the stepwise sulfurization detailed in Figure 4E. MoO_3 vapor reacts with sulfur vapor to first form MoO_2, which is further sulfurized to form $MoOS_2$ crystals. These intermediate $MoOS_2$ crystals can be vaporized, further sulfurized, and then recrystallized as MoS_2 nearby. This is consistent with reported conversion of MoO_2 nanocrystals into MoS_2 via CVD sulfurization.[53] The SiO_2 growth substrates used in growth of these species are amorphous, so we investigated the sulfurization of MoO_3 using crystalline fluorophlogopite (mica) substrates. Using molar loading ratios of 0.2:1, 8:1, and greater than 200:1, we selectively grew MoO_2, $MoOS_2$, and MoS_2 on mica (Figure S8), suggesting that the stepwise sulfurization of MoO_3 to MoS_2 is applicable to both amorphous and crystalline growth substrates. Our experiments demonstrate that it is essential to maintain a S:Mo ratio of 3.5:1 at the substrate surface during the entire growth process in order to bypass this stepwise growth pathway. While there likely exists a minimum S:Mo loading ratio required to push reaction 1 to completion, we did not determine this ratio. Due to the complexity of the CVD growth

DOI: 10.1021/acsanm.8b01266
ACS Appl. Nano Mater. 2018, 1, 5655−5661

process, any optimized loading ratio would only apply to a specific set of growth conditions and would not easily translate to a different CVD apparatus.

An S:Mo loading ratio greater than 1500:1 maintained excess sulfur to selectively grow MoS_2. Sulfur was held at room temperature and moved into a 250 °C zone to vaporize only when the center of the furnace reached 650 °C, ensuring a constant supply of sulfur vapor to maintain a stable S:Mo ratio across the substrate during the entirety of the growth. A short growth time was used to synthesize triangular crystals of MoS_2 rather than continuous films which form from merged crystals.[19,22,27,38] Optical microscopy and SEM analysis of the resulting crystals reveal that they are triangular with clean edges (Figure 5A,B). Raman and XPS characterization of these

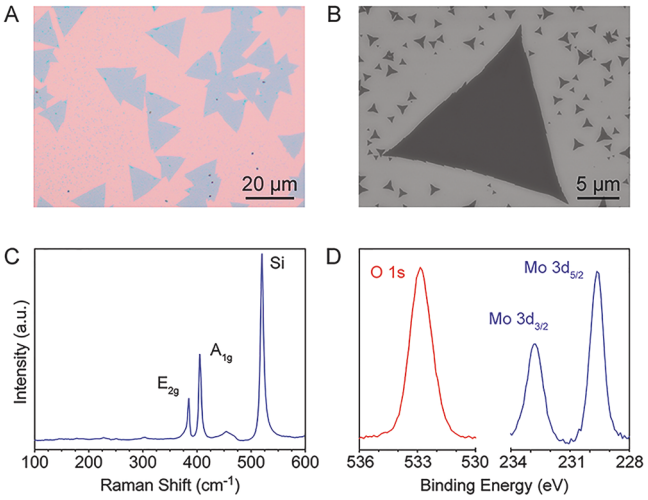

Figure 5. Characterization of MoS_2 crystals grown in excess sulfur. (A) Optical image of triangular MoS_2 crystals. The purple crystals are monolayer; however, some small blue regions indicate the beginning of multilayer growth on some crystals. (B) SEM image of the triangular crystals shown in (A). (C) Raman spectrum of the triangular crystals in (A) showing the E_{2g} and A_{1g} peaks of MoS_2. The peak at 520 cm^{-1} corresponds to the Si growth substrate. (D) XPS spectra of the O 1s (left) and Mo 3d (right) peaks from the crystals in (A).

crystals confirms they are chemically pure MoS_2 (Figures 5C,D and S9),[46,61] with no presence of $MoOS_2$.[58,59] The 20 cm^{-1} separation of the E_{2g} and A_{1g} peaks (Figure S9B) is consistent with reported values for monolayer CVD-grown MoS_2.[35,37]

CONCLUSIONS

In summary, we report the stepwise sulfurization of MoO_3 to form MoS_2 via chemical vapor deposition. By controlling the local and global S:Mo molar ratio present in the gas-phase at the growth substrate surface, we have demonstrated that MoO_3 can be sulfurized to form MoO_2, then $MoOS_2$, and finally MoS_2 as a function of increasing sulfur vapor concentration. Characterization of $MoOS_2/MoS_2$ hybrid crystals and observation of the direct conversion of $MoOS_2$ crystals into MoS_2 reveal that $MoOS_2$ serves as an intermediate in the formation of MoS_2 and provide direct evidence for a stepwise sulfurization process. This mechanism underlines the importance of keeping sulfur in excess throughout CVD growth in order to synthesize chemically pure MoS_2, rather than the intermediate products. The increasing applications and interest in MoS_2 is creating a demand for synthesis techniques offering control over thickness, morphology, and purity, necessitating further work to develop reproducible and robust chemical vapor deposition techniques.

EXPERIMENTAL METHODS

Chemical Vapor Deposition Synthesis of $MoOS_2$ and MoS_2. MoS_2 and $MoOS_2$ were synthesized inside a quartz tube (1 in. OD) placed in a Lindberg-Blue Mini-Mite single-zone tube furnace (ThermoFisher). Sulfur powder (99.5%, Alfa Aesar) was placed in a quartz holder that was placed 17.5 cm upstream of the center of the furnace. MoO_3 powder (99.97%, Sigma-Aldrich) was spread out over approximately a 1 cm region in a separate quartz holder, placed at the center of the furnace. Growth substrates of 300 nm SiO_2 on silicon were cut into 3 cm^2 sections and sonicated for 5 min each in acetone, isopropanol, and distilled H_2O. Substrates were then plasma cleaned for 5 min with an air plasma. Cleaned substrates were then placed face-down on top of the quartz holder directly above the MoO_3 powder. Substrates were placed 1−2 cm downstream of the MoO_3 powder only for the experiments investigating the effect of substrate placement (Figure 1).

The quartz tube was purged with argon gas (99.998% by volume, Airgas) for a minimum of 10 min at atmospheric pressure to remove oxygen. The argon gas was continuously flowed through the tube throughout the entire synthesis process at a flow rate ranging from 70 sccm to 100 sccm. The furnace was heated to a growth temperature of 650 °C at a rate of 15 °C per minute and then held at temperature for 10−20 min. During growth, the MoO_3 and substrate remained in a stable zone of 650 °C and the sulfur was held in a 250 °C zone 17.5 cm upstream. The furnace was then allowed to cool slowly to 400−300 °C and then opened to cool more rapidly to room temperature.

Sulfurization of $MoOS_2$ Crystals. Substrates with CVD-grown $MoOS_2$ were placed in a quartz tube placed in the center of a single-zone furnace. Sulfur (2.0 g) was placed in a 3 mL alumina combustion boat (CoorsTek) with the leading edge of the boat 19 cm upstream of the center of the furnace with a magnet placed further upstream of the combustion boat. The furnace was purged with 35 sccm of argon gas for 10 min and then heated to 630 °C at 15 °C per minute under argon gas flow. Sulfur was then pushed with the magnet to a 250 °C zone 17.5 cm upstream of the MoO_3. The furnace was further heated for 5 min yielding a temperature of 700 °C in the center and 275 °C 17.5 cm upstream. The furnace was then held at temperature for 10 min before being allowed to cool to room temperature.

Synthesis of Triangular MoS_2 Crystals. Sulfur powder (1.5 g) was placed in a 3 mL alumina combustion boat with the leading edge of the boat 19 cm upstream of the center of the furnace with a magnet placed further upstream of the combustion boat. MoO_3 powder (3.2 mg) was placed in a quartz holder with a substrate placed 12 mm directly above the MoO_3. The substrate was cleaned as described above and then treated with 2−5 μL of 10 μM aqueous hexamethylpararosaniline chloride (crystal violet, >90%, Sigma-Aldrich) spread out onto the surface with the side of a pipet tip and allowed to air-dry. The furnace was purged with 35 sccm of argon gas for 10 min and then heated to 650 °C at 15 °C per minute under argon gas flow. Sulfur was then pushed with the magnet to a 250 °C zone 17.5 cm upstream of the MoO_3. The furnace was further heated for 3 min yielding a temperature of 700 °C in the center and 275 °C 17.5 cm upstream. The furnace was then held at temperature for 5 min before being allowed to cool to room temperature.

Characterization. Optical images were taken with an Olympus BX51 microscope. Scanning electron micrographs were taken with a Hitachi SU8230 CFE SEM using a 10 kV accelerating voltage. Raman spectra were taken with a Horiba LabRAM HR Evolution spectrometer using a 2.5 mW 532 nm laser. The Raman peak of crystalline silicon at 520 cm^{-1} was used as an internal standard for all Raman spectra. The X-ray photoelectron spectra were collected using a monochromatic 1486.7 eV Al Kα X-ray source on a PHI VersaProbe II X-ray photoelectron spectrometer with a 0.47 eV system resolution. The energy scale was calibrated using Cu $2p_{3/2}$ (932.67 eV) and Au $4f_{7/2}$ (84.00 eV) peaks on a clean copper plate and clean gold foil.

DOI: 10.1021/acsanm.8b01266
ACS Appl. Nano Mater. 2018, 1, 5655−5661

XPS spectra were normalized using the adventitious carbon C 1s peak at 284.5 eV. Atomic force microscopy images were taken with a Bruker Dimension Fastscan atomic force microscope using Fastscan B AFM tips (Bruker) at a scanning rate of 0.5−1.0 Hz.

■ ASSOCIATED CONTENT

Supporting Information

The Supporting Information is available free of charge on the ACS Publications website at DOI: 10.1021/acsanm.8b01266.

Growth parameters for MoS_2, Raman spectra from standards of the reactants and products in the CVD growth of MoS_2, characterization of MoS_2 films grown under vacuum at 800 °C with different sulfur concentrations, XPS characterization of $MoOS_2/MoS_2$ hybrid crystals, characterization of $MoOS_2/MoS_2$ hybrid crystals grown under a S:Mo molar loading ratio of 17:1, AFM characterization of hybrid $MoOS_2/MoS$, Raman characterization of $MoOS_2$ crystals sulfurized in the absence of Mo precursor, characterization of MoO_2, $MoOS_2$, and MoS_2 grown on crystalline mica, characterization of MoS_2 crystals grown in excess sulfur, and identification of Raman modes present in spectra of MoO_2, $MoOS_2$, and MoS_2 (PDF)

■ AUTHOR INFORMATION

Corresponding Author

*E-mail: judy.cha@yale.edu.

ORCID

Joshua V. Pondick: 0000-0003-3380-2686

John M. Woods: 0000-0003-2546-893X

Judy J. Cha: 0000-0002-6346-2814

Notes

The authors declare no competing financial interest.

[⊥]J.J.C. is a Canadian Institute for Advanced Research Azrieli Global Scholar.

■ ACKNOWLEDGMENTS

This work was supported by NSF EFMA Grant 1542815 and the Canadian Institute for Advanced Research (CIFAR) Global Scholars Quantum Materials Program. Spectroscopy and microscopy facilities were supported by the Yale West Campus Materials Characterization Core (MCC) and the Yale Institute for Nanoscience and Quantum Engineering (YINQE).

■ REFERENCES

(1) Kim, S.; Konar, A.; Hwang, W.-S.; Lee, J. H.; Lee, J.; Yang, J.; Jung, C.; Kim, H.; Yoo, J.-B.; Choi, J.-Y.; et al. High-Mobility and Low-Power Thin-Film Transistors Based on Multilayer MoS_2 Crystals. *Nat. Commun.* **2012**, *3*, 1011.

(2) Radisavljevic, B.; Radenovic, A.; Brivio, J.; Giacometti, V.; Kis, A. Single-Layer MoS_2 Transistors. *Nat. Nanotechnol.* **2011**, *6*, 147−150.

(3) Chhowalla, M.; Jena, D.; Zhang, H. Two-Dimensional Semiconductors for Transistors. *Nat. Rev. Mater.* **2016**, *1*, 16052.

(4) Lee, H. S.; Min, S. W.; Chang, Y. G.; Park, M. K.; Nam, T.; Kim, H.; Kim, J. H.; Ryu, S.; Im, S. MoS_2 Nanosheet Phototransistors with Thickness-Modulated Optical Energy Gap. *Nano Lett.* **2012**, *12*, 3695−3700.

(5) Wang, Q. H.; Kalantar-zadeh, K.; Kis, A.; Coleman, J. N.; Strano, M. S. Electronics and Optoelectronics of Two-Dimensional Transition Metal Dichalcogenides. *Nat. Nanotechnol.* **2012**, *7*, 699−712.

(6) Mak, K. F.; Shan, J. Photonics and Optoelectronics of 2D Semiconductor Transition Metal Dichalcogenides. *Nat. Photonics* **2016**, *10*, 216−226.

(7) Hinnemann, B.; Moses, P. G.; Bonde, J.; Jørgensen, K. P.; Nielsen, J. H.; Horch, S.; Chorkendorff, I.; Nørskov, J. K. Biomimetic Hydrogen Evolution: MoS_2 Nanoparticles as Catalyst for Hydrogen Evolution. *J. Am. Chem. Soc.* **2005**, *127*, 5308−5309.

(8) Jaramillo, T. F.; Jorgensen, K. P.; Bonde, J.; Nielsen, J. H.; Horch, S.; Chorkendorff, I. Identification of Active Edge Sites for Electrochemical H_2 Evolution from MoS_2 Nanocatalysts. *Science* **2007**, *317*, 100−102.

(9) Voiry, D.; Fullon, R.; Yang, J.; de Carvalho Castro e Silva, C.; Kappera, R.; Bozkurt, I.; Kaplan, D.; Lagos, M. J.; Batson, P. E.; Gupta, G.; et al. The Role of Electronic Coupling between Substrate and 2D MoS_2 Nanosheets in Electrocatalytic Production of Hydrogen. *Nat. Mater.* **2016**, *15*, 1003−1009.

(10) Zhou, Y.; Silva, J. L.; Woods, J. M.; Pondick, J. V.; Feng, Q.; Liang, Z.; Liu, W.; Lin, L.; Deng, B.; Brena, B.; et al. Revealing the Contribution of Individual Factors to Hydrogen Evolution Reaction Catalytic Activity. *Adv. Mater.* **2018**, *30*, 1706076.

(11) Splendiani, A.; Sun, L.; Zhang, Y.; Li, T.; Kim, J.; Chim, C. Y.; Galli, G.; Wang, F. Emerging Photoluminescence in Monolayer MoS_2. *Nano Lett.* **2010**, *10*, 1271−1275.

(12) Mak, K. F.; Lee, C.; Hone, J.; Shan, J.; Heinz, T. F. Atomically Thin MoS_2: A New Direct-Gap Semiconductor. *Phys. Rev. Lett.* **2010**, *105*, 2−5.

(13) Joensen, P.; Frindt, R. F.; Morrison, S. R. Single-Layer MoS_2. *Mater. Res. Bull.* **1986**, *21*, 457−461.

(14) Heising, J.; Kanatzidis, M. G. Structure of Restacked MoS_2 and WS_2 Elucidated by Electron Crystallography. *J. Am. Chem. Soc.* **1999**, *121*, 638−643.

(15) Coleman, J. N.; Lotya, M.; O'Neill, A.; Bergin, S. D.; King, P. J.; Khan, U.; Young, K.; Gaucher, A.; De, S.; Smith, R. J.; et al. Two-Dimensional Nanosheets Produced by Liquid Exfoliation of Layered Materials. *Science* **2011**, *331*, 568−571.

(16) Nicolosi, V.; Chhowalla, M.; Kanatzidis, M. G.; Strano, M. S.; Coleman, J. N. Liquid Exfoliation of Layered Materials. *Science* **2013**, *340*, 72−75.

(17) Fu, D.; Zhao, X.; Zhang, Y.-Y.; Li, L.; Xu, H.; Jang, A.-R.; Yoon, S. I.; Song, P.; Poh, S. M.; Ren, T.; et al. Molecular Beam Epitaxy of Highly Crystalline Monolayer Molybdenum Disulfide on Hexagonal Boron Nitride. *J. Am. Chem. Soc.* **2017**, *139*, 9392−9400.

(18) Zhan, Y.; Liu, Z.; Najmaei, S.; Ajayan, P. M.; Lou, J. Large-Area Vapor-Phase Growth and Characterization of MoS_2 Atomic Layers on a SiO_2 Substrate. *Small* **2012**, *8*, 966−971.

(19) Lee, Y. H.; Zhang, X. Q.; Zhang, W.; Chang, M. T.; Lin, C. Te; Chang, K. Di; Yu, Y. C.; Wang, J. T. W.; Chang, C. S.; Li, L. J.; et al. Synthesis of Large-Area MoS_2 Atomic Layers with Chemical Vapor Deposition. *Adv. Mater.* **2012**, *24*, 2320−2325.

(20) Yu, Y.; Li, C.; Liu, Y.; Su, L.; Zhang, Y.; Cao, L. Controlled Scalable Synthesis of Uniform, High-Quality Monolayer and Few-Layer MoS_2 Films. *Sci. Rep.* **2013**, *3*, 1866.

(21) Choudhary, N.; Park, J.; Hwang, J. Y.; Choi, W. Growth of Large-Scale and Thickness-Modulated MoS_2 Nanosheets. *ACS Appl. Mater. Interfaces* **2014**, *6*, 21215−21222.

(22) Wang, S.; Pacios, M.; Bhaskaran, H.; Warner, J. H. Substrate Control for Large Area Continuous Films of Monolayer MoS_2 by Atmospheric Pressure Chemical Vapor Deposition. *Nanotechnology* **2016**, *27*, 085604.

(23) Yu, H.; Liao, M.; Zhao, W.; Liu, G.; Zhou, X. J.; Wei, Z.; Xu, X.; Liu, K.; Hu, Z.; Deng, K.; et al. Wafer-Scale Growth and Transfer of Highly-Oriented Monolayer MoS_2 Continuous Films. *ACS Nano* **2017**, *11*, 12001−12007.

(24) Bilgin, I.; Liu, F.; Vargas, A.; Winchester, A.; Man, M. K. L.; Upmanyu, M.; Dani, K. M.; Gupta, G.; Talapatra, S.; Mohite, A. D.; et al. Chemical Vapor Deposition Synthesized Atomically Thin Molybdenum Disulfide with Optoelectronic-Grade Crystalline Quality. *ACS Nano* **2015**, *9*, 8822−8832.

(25) Tu, Z.; Li, G.; Ni, X.; Meng, L.; Bai, S.; Chen, X.; Lou, J.; Qin, Y. Synthesis of Large Monolayer Single Crystal MoS_2 Nanosheets with Uniform Size through a Double-Tube Technology. *Appl. Phys. Lett.* **2016**, *109*, 223101.
(26) Kurabayashi, S.; Nagashio, K. Transport Properties of the Top and Bottom Surfaces in Monolayer MoS_2 Grown by Chemical Vapor Deposition. *Nanoscale* **2017**, *9* (35), 13264.
(27) van der Zande, A. M.; Huang, P. Y.; Chenet, D. A.; Berkelbach, T. C.; You, Y.; Lee, G.-H.; Heinz, T. F.; Reichman, D. R.; Muller, D. A.; Hone, J. C. Grains and Grain Boundaries in Highly Crystalline Monolayer Molybdenum Disulphide. *Nat. Mater.* **2013**, *12*, 554−561.
(28) Wu, S.; Huang, C.; Aivazian, G.; Ross, J. S.; Cobden, D. H.; Xu, X. Vapor-Solid Growth of High Optical Quality MoS_2 Monolayers with near-Unity Valley Polarization. *ACS Nano* **2013**, *7*, 2768−2772.
(29) Lee, Y. H.; Yu, L.; Wang, H.; Fang, W.; Ling, X.; Shi, Y.; Lin, C. Te; Huang, J. K.; Chang, M. T.; Chang, C. S.; et al. Synthesis and Transfer of Single-Layer Transition Metal Disulfides on Diverse Surfaces. *Nano Lett.* **2013**, *13*, 1852−1857.
(30) Li, S.; Lin, Y.; Zhao, W.; Wu, J.; Wang, Z.; Hu, Z.; Shen, Y.; Tang, D.; Wang, J.; Zhang, Q.; et al. Vapour−Liquid−Solid Growth of Monolayer MoS_2 Nanoribbons. *Nat. Mater.* **2018**, *17*, 535−543.
(31) Zhou, J.; Lin, J.; Huang, X.; Zhou, Y.; Chen, Y.; Xia, J.; Wang, H.; Xie, Y.; Yu, H.; Lei, J.; et al. A Library of Atomically Thin Metal Chalcogenides. *Nature* **2018**, *556*, 355−359.
(32) Dahl-Petersen, C.; Saric, M.; Brorson, M.; Moses, G.; Rossmeisl, J.; Lauritsen, J. V.; Helveg, S. Topotactic Growth of Edge-Terminated MoS_2 from MoO_2 Nanocrystals. *ACS Nano* **2018**, *12*, 5351−5358.
(33) Li, L.; Long, R.; Prezhdo, O. V. Why Chemical Vapor Deposition Grown MoS2 Samples Outperform Physical Vapor Deposition Samples: Time-Domain ab Initio Analysis. *Nano Lett.* **2018**, *18*, 4008−4014.
(34) Najmaei, S.; Liu, Z.; Zhou, W.; Zou, X.; Shi, G.; Lei, S.; Yakobson, B. I.; Idrobo, J.-C.; Ajayan, P. M.; Lou, J. Vapour Phase Growth and Grain Boundary Structure of Molybdenum Disulphide Atomic Layers. *Nat. Mater.* **2013**, *12*, 754−759.
(35) Wang, S.; Rong, Y.; Fan, Y.; Pacios, M.; Bhaskaran, H.; He, K.; Warner, J. H. Shape Evolution of Monolayer MoS_2 Crystals Grown by Chemical Vapor Deposition. *Chem. Mater.* **2014**, *26*, 6371−6379.
(36) Xie, S.; Xu, M.; Liang, T.; Huang, G.; Wang, S.; Xue, G.; Meng, N.; Xu, Y.; Chen, H.; Ma, X.; et al. A High-Quality Round-Shaped Monolayer MoS_2 Domain and Its Transformation. *Nanoscale* **2016**, *8*, 219−225.
(37) Ling, X.; Lee, Y. H.; Lin, Y.; Fang, W.; Yu, L.; Dresselhaus, M. S.; Kong, J. Role of the Seeding Promoter in MoS_2 Growth by Chemical Vapor Deposition. *Nano Lett.* **2014**, *14*, 464−472.
(38) Senthilkumar, V.; Tam, L. C.; Kim, Y. S.; Sim, Y.; Seong, M. J.; Jang, J. I. Direct Vapor Phase Growth Process and Robust Photoluminescence Properties of Large Area MoS_2 Layers. *Nano Res.* **2014**, *7*, 1759−1768.
(39) Lim, Y. F.; Priyadarshi, K.; Bussolotti, F.; Gogoi, P. K.; Cui, X.; Yang, M.; Pan, J.; Tong, S. W.; Wang, S.; Pennycook, S. J.; et al. Modification of Vapor Phase Concentrations in MoS_2 Growth Using a NiO Foam Barrier. *ACS Nano* **2018**, *12*, 1339−1349.
(40) Li, X. L.; Li, Y. D. Formation of MoS_2 Inorganic Fullerenes (IFs) by the Reaction of MoO_3 Nanobelts and S. *Chem. - Eur. J.* **2003**, *9*, 2726−2731.
(41) Arnoldy, P.; van den Heijkant, J. A. M.; De Bok, G. D.; Moulijn, J. A. Temperature-Programmed Sulfiding of MoO_3/Al_2O_3 Catalysts. *J. Catal.* **1985**, *92*, 35−55.
(42) Okamoto, Y.; Kato, A.; Usman; Rinaldi, N.; Fujikawa, T.; Koshika, H.; Hiromitsu, I.; Kubota, T. Effect of Sulfidation Temperature on the Intrinsic Activity of Co-MoS_2 and Co-WS_2 Hydrodesulfurization Catalysts. *J. Catal.* **2009**, *265*, 216−228.
(43) Wu, Z.; Wang, D.; Sun, A. Preparation of MoS_2 Nanoflakes by a Novel Mechanical Activation Method. *J. Cryst. Growth* **2010**, *312*, 340−343.
(44) Muijsers, J. C.; Weber, T.; Vanhardeveld, R. M.; Zandbergen, H. W.; Niemantsverdriet, J. W. Sulfidation Study of Molybdenum Oxide Using $MoO_3/SiO_2/Si(100)$ Model Catalysts and Mo^{IV}_3-Sulfur Cluster Compounds. *J. Catal.* **1995**, *157*, 698−705.
(45) Weber, T.; Muijsers, J. C.; van Wolput, J. H. M. C.; Verhagen, C. P. J.; Niemantsverdriet, J. W. Basic Reaction Steps in the Sulfidation of Crystalline MoO_3 to MoS_2 as Studied by X-Ray Photoelectron and Infrared Emission Spectroscopy. *J. Phys. Chem.* **1996**, *100*, 14144−14150.
(46) Li, S. L.; Miyazaki, H.; Song, H.; Kuramochi, H.; Nakaharai, S.; Tsukagoshi, K. Quantitative Raman Spectrum and Reliable Thickness Identification for Atomic Layers on Insulating Substrates. *ACS Nano* **2012**, *6*, 7381−7388.
(47) Lee, C.; Yan, H.; Brus, L.; Heinz, T.; Hone, J.; Ryu, S. Anomalous Lattice Vibrations of Single-and Few-Layer MoS2. *ACS Nano* **2010**, *4*, 2695−2700.
(48) Wu, H.; Zhou, X.; Li, J.; Li, X.; Li, B.; Fei, W.; Zhou, J.; Yin, J.; Guo, W. Ultrathin Molybdenum Dioxide Nanosheets as Uniform and Reusable Surface-Enhanced Raman Spectroscopy Substrates with High Sensitivity. *Small* **2018**, *14*, 1802276.
(49) Schrader, G. L.; Cheng, C. P. In Situ Laser Raman Spectroscopy of the Sulfiding of $MO/\gamma\text{-}A1_2O_3$ Catalysts. *J. Catal.* **1983**, *80*, 369−385.
(50) Dieterle, M.; Mestl, G. Raman Spectroscopy of Molybdenum Oxides. *Phys. Chem. Chem. Phys.* **2002**, *4*, 822−826.
(51) Camacho-López, M. A.; Escobar-Alarcón, L.; Picquart, M.; Arroyo, R.; Córdoba, G.; Haro-Poniatowski, E. Micro-Raman Study of the m-MoO_2 to α-MoO_3 transformation Induced by cw-Laser Irradiation. *Opt. Mater.* **2011**, *33*, 480−484.
(52) Çakır, D.; Peeters, F. M.; Sevik, C. Mechanical and Thermal Properties of *h* -MX_2 (M = Cr, Mo, W; X = O, S, Se, Te) Monolayers: A Comparative Study. *Appl. Phys. Lett.* **2014**, *104*, 203110.
(53) Wang, X.; Feng, H.; Wu, Y.; Jiao, L. Controlled Synthesis of Highly Crystalline MoS_2 Flakes by Chemical Vapor Deposition. *J. Am. Chem. Soc.* **2013**, *135*, 5304−5307.
(54) Solferino, G.; Anderson, A. J. Thermal Reduction of Molybdite and Hematite in Water and Hydrogen Peroxide-Bearing Solutions: Insights on Redox Conditions in Hydrothermal Diamond Anvil Cell (HDAC) Experiments. *Chem. Geol.* **2012**, *322*−*323*, 215−222.
(55) Srivastava, R.; Chase, L. L. Raman Spectra of CrO_2 and MoO_2 Single Crystals. *Solid State Commun.* **1972**, *11*, 349−353.
(56) Dang, T. A.; Chau, C. N. Electron Spectroscopy for Chemical Analysis of Cool White Phosphors Coated with SiO_2 Thin Film. *J. Electrochem. Soc.* **1996**, *143*, 302−305.
(57) Anwar, M.; Hogarth, C.; Bulpett, R. Effect of Substrate Temperature and Film Thickness on the Surface Structure of Some Thin Amorphous Films of MoO_3 Studied by X-Ray Photoelectron Spectroscopy (ESCA). *J. Mater. Sci.* **1989**, *24*, 3087−3090.
(58) Benoist, L.; Gonbeau, D.; Pfister-Guillouzo, G.; Schmidt, E.; Meunier, G.; Levasseur, A. X-Ray Photoelectron Spectroscopy Characterization of Amorphous Molybdenum Oxysulfide Thin Films. *Thin Solid Films* **1995**, *258*, 110−114.
(59) Qiao, Y.; Hu, X.; Liu, Y.; Liang, G.; Croft, M. C.; Huang, Y. Surface Modification of MoO_xS_y on Porous TiO_2 Nanospheres as an Anode Material with Highly Reversible and Ultra-Fast Lithium Storage Properties. *J. Mater. Chem. A* **2013**, *1*, 15128.
(60) Wu, C. R.; Chang, X. R.; Wu, C. H.; Lin, S. Y. The Growth Mechanism of Transition Metal Dichalcogenides by Using Sulfurization of Pre-Deposited Transition Metals and the 2D Crystal Hetero-Structure Establishment. *Sci. Rep.* **2017**, *7*, 42146.
(61) Lin, Y.-C.; Lu, N.; Perea-Lopez, N.; Li, J.; Lin, Z.; Peng, X.; Lee, C. H.; Sun, C.; Calderin, L.; Browning, P. N.; et al. Direct Synthesis of van Der Waals Solids. *ACS Nano* **2014**, *8*, 3715−3723.

DOI: 10.1021/acsanm.8b01266
ACS Appl. Nano Mater. 2018, 1, 5655−5661